BULLETIN DE L'ASSOCIATION MINÉRALOGIQUE DU CANADA

THE CANADIAN MINERALOGIST

JOURNAL OF THE MINERALOGICAL ASSOCIATION OF CANADA

Volume 37 October 1999 Part 5

The Canadian Mineralogist
Vol. 37, pp. 1081-1097 (1999)

PLATINUM-GROUP ELEMENTS AND GOLD IN Cu–Ni-MINERALIZED PERIDOTITE AT GABBRO AKAREM, EASTERN DESERT, EGYPT

NADIA A. SHARARA

Department of Geology, Faculty of Science, Assiut University, Assiut, 71516, Egypt

GRAHAM C. WILSON[§] AND JOHN C. RUCKLIDGE

Isotrace Laboratory at the University of Toronto, 60 St. George Street, Toronto, Ontario M5T 2T3, Canada

ABSTRACT

The Akarem mafic–ultramafic complex is located at 24°01'N, 34°08'E, 130 km east of Aswan, in the southern part of the Eastern Desert of Egypt. The late Proterozoic complex includes an earlier, mostly layered, gabbroic phase and a later peridotite phase. The latter was emplaced in two successive stages, with barren followed by mineralized (Cu–Ni sulfide-bearing) peridotites. The gabbroic rocks are largely gabbronorite, olivine gabbronorite, troctolite and hornblende gabbro. Unmineralized peridotite is lherzolite, whereas the mineralized peridotite is dunite and harzburgite. The rocks are highly serpentinized. The estimated mode of the mineralized peridotite includes ≤35% olivine, 15% serpentine, ≤3% plagioclase, 16% clinopyroxene, 4% orthopyroxene, 6% amphibole, ≤15% pyrrhotite, ≤3% pentlandite and 3% chalcopyrite. The reserves in mineralized peridotite above 130 m depth have been inferred to be ~700,000 tonnes. The primary sulfides are pyrrhotite, pentlandite, chalcopyrite and cubanite. These minerals exhibit disseminated, massive and net textures in the olivine-rich ultramafic cumulate host. Secondary minerals include violarite, pyrite, monoclinic pyrrhotite, magnetite, mackinawite and millerite. Analyses of bulk rocks and selected coarse sulfide grains were made by a combination of techniques, including instrumental neutron activation (INAA) and inductively coupled plasma – mass spectrometry (ICP–MS), electron-probe micro-analysis (EPMA) and accelerator mass spectrometry (AMS). S/Se ratios and $\delta^{34}S$ values of the sulfide-rich rocks, although not a definitive proof, are consistent with a magmatic S source with minimal crustal contamination. *In situ* Au levels measured by AMS are low: pyrrhotite contains 2–25 ppb, pentlandite 3–8 ppb and chalcopyrite 2–8 ppb. These values are much below bulk-rock levels (60–1080 ppb). Trace Pt (<2 ppb) is detected in the sulfides, also far below bulk levels (20–330 ppb). Coarse pyrrhotite carries more Rh (20–120 ppb, mean 60 ppb) than bulk rock (mean 20 ppb) and other major sulfides. Ir is similar; other sulfides and bulk samples carry much less (a few ppb) than coarse pyrrhotite (30–100 ppb, mean 60 ppb). Coarse granular pentlandite has the highest Pd contents, up to 1030 ppb. Mass-balance calculations suggest that most Au and Pt probably form discrete grains of native Au and PGM. In contrast, most of the Pd, Rh and Ir is present within Fe–Ni–Cu sulfides, probably incorporated in the lattice of their host(s). PGE distributions can be explained by fractional crystallization of *mss* from parental sulfide liquid.

Keywords: mafic–ultramafic rocks, magmatic sulfide, nickel, copper, mineralization, ore textures, platinum-group elements (PGE), gold, electron microprobe, accelerator mass spectrometry, sulfur isotopes, S/Se ratios, ore genesis, Eastern Desert, Egypt.

§ *E-mail address*: gcw@quartz.geology.utoronto.ca

Sommaire

Le complexe mafique–ultramafique d'Akarem, d'âge protérozoïque supérieur, est situé à 130 km à l'est d'Aswan, dans la partie méridionale du Désert de l'Est de l'Égypte. Le complexe d'Akarem comprend une phase gabbroïque initiale, principalement stratifiée, et une phase tardive péridotitique, elle-même divisée en une unité de base dépourvue de minerai suivie d'une unité minéralisée en sulfures de nickel et de cuivre. La péridotite dépourvue de sulfures est une lherzolite, alors que les roches bien minéralisées sont dunitiques et harzburgitiques. Les roches ultramafiques sont fortement serpentinisées. Les sulfures principaux sont la pyrrhotite, la pentlandite, la chalcopyrite, et la cubanite. Ces minéraux présentent des textures disséminées, massives, et réticulaires dans les cumulats ultramafiques riches en olivine. Parmi les minéraux secondaires, on trouve violarite, pyrite, pyrrhotite monoclinique, magnétite, mackinawite, et millerite. Les analyses chimiques des roches et de certain sulfures à grain grossiers ont été effectuées avec une combinaison de techniques, y inclus: activation neutronique (INAA), spectrométrie de masse, analyses à la microsonde électronique et par accélérateur avec spectrométrie de masse (AMS). Bien que n'offrant pas une preuve définitive, le rapport S/Se et les valeurs isotopiques du soufre des roches enrichies en sulfures semblent indiquer une source magmatique du soufre, avec une contamination minimale par la croûte. Les concentrations d'or "in situ" obtenues par AMS sont faibles. La pyrrhotite contient de 2 à 25 ppb d'or, la pentlandite, de 3 à 8 ppb, et la chalcopyrite, de 2 à 8 ppb. Ces teneurs sont de beaucoup inférieures aux teneurs des roches globales (60 à 1080 ppb). De même, des teneurs en Pt à l'état de traces (< 2 ppb) ont été détectées dans les sulfures, bien en dessous des teneurs des roches entières (20–330 ppb). La pyrrhotite à grains grossiers contient plus de Rh (30–120 ppb, moyenne 60 ppb) que les roches globales (moyenne 20 ppb), et les autres sulfures principaux. Il en est de même pour Ir; les autres sulfures et les roches globales en contiennent bien moins (quelque ppb) que la pyrrhotite à grain grossier (30–100 ppb, moyenne 60 ppb). La pentlandite grenue à grains grossiers possède la concentration de Pd la plus élevée, jusqu'à 1030 ppb. D'après les calculs normatifs, la plupart de l'or et du platine se trouverait probablement sous forme de grains d'or natif et de minéraux du groupe du platine. En revanche, la plupart du Pd, Rh, et Ir serait présent dans les sulfures de Fe–Ni–Cu, probablement dans leur structure. La distribution des éléments du groupe du platine resulterait de la cristallisation fractionnée d'une solution solide monosulfurée (*mss*) à partir du liquide sulfuré.

Mots-clés: roches mafiques–ultramafiques, minéralisation, sulfures magmatiques, nickel, cuivre, textures du minerai, éléments du groupe du platine (EGP), or, microsonde électronique, spectrométrie de masse par accélérateur, isotopes du soufre, rapports S/Se, origine, Désert de l'Est, Egypte.

Introduction

The objective of this study is to investigate the processes of formation of the Ni–Cu mineralization at Gabbro Akarem, in the Eastern Desert of Egypt, with particular reference to the precious-metal contents of the sulfide-rich mafic–ultramafic rocks. In this article, we describe the distribution of platinum-group elements (PGE) in the sulfide minerals and illustrate the geochemical behavior of the PGE during the process of sulfide accumulation.

The problem of the heterogeneous distribution of the PGE, both dispersed in common sulfides and localized in rare, discrete platinum-group minerals (PGM), is addressed by a combination of techniques: ore microscopy, electron-microprobe analysis and accelerator mass spectrometry (AMS). The AMS technique applied here permits the detection of heavy elements down to ppb levels in single grains with a minimum diameter of ~0.5 mm in polished samples. Despite its limited spatial resolution, AMS is the most sensitive *in situ* technique available for this type of study, and is applicable to coarse assemblages of ore minerals.

The Gabbro Akarem intrusion has been the focus of a number of studies in the past 25 years (Carter 1975, Rasmy 1982a, b, Hafez & Abdel-Kader 1982, Bishady *et al.* 1991, Khudeir *et al.* 1996, El Sideck & El Goresy 1996, El Mahalawy & Helmy 1997, Helmy *et al.* 1998). The present work seems to be the first detailed attempt to document the PGE and Au contents of the sulfide deposits and evaluate their economic potential.

Local Geology and Regional Setting

Introduction

The Gabbro Akarem mafic–ultramafic intrusion is located 130 km east of Aswan town in the southern part of the Eastern Desert of Egypt, at 24°01'N, 34°08'E (Fig. 1). The complex consists of two dyke-like bodies 1.5 km apart, and extends over a distance of 11 km in an ENE direction. It was emplaced along an active fault trending ENE–WSW. The smaller western body is 0.5 km wide and 2.5 km in length. The main (eastern) body is ~7.5 km long and 1–2 km wide, although fault offsets obscure the true width. Most of the intrusions are covered by overburden and gossans, with secondary Cu–Ni minerals the key criterion for locating showings. The sulfide concentrations can be traced along the surface as outcrops of gossan in zones 0.5–1.5 km in length. In these zones, the individual gossans range from 0.1 m to 1 m in thickness and from 1 m to 30 m in length. Trenching proved that these separate outcrops generally form much longer zones obscured by a cover of eluvial material only 10 to 20 cm thick (Fig. 2).

Mapping and exploration of the Akarem mafic–ultramafic intrusions were previously carried out through the UNDP (United Nations Development Programme)

in 1974. The two bodies were intruded into Proterozoic paragneisses of semipelitic composition and cut in turn by later calc-alkaline granodiorite to diorite bodies. The Gabbro Akarem complex is composed of an older, mostly layered gabbroic phase intruded by younger peridotites. The gabbroic and peridotitic masses are variously marked and cut by conformable layers and lenticles and later dykes of pyroxenite. The gabbro mass is composed largely of gabbronorites that grade, with increasing proportions of olivine or hornblende, into either olivine gabbronorite and troctolite or hornblende gabbro. The peridotites comprise two phases, an earlier lherzolite grading into melagabbronorite with increasing plagioclase, and a later phase of wehrlite and harzburgite to which the massive, network-type and disseminated magmatic Cu–Ni sulfide mineralization is confined. The pyroxenite comprises olivine orthopyroxenite and olivine websterite; it represents a later suite of dyke-like bodies introduced during and after the emplacement of the mineralized peridotite. The peridotite represents the footwall, whereas the layered gabbros are the hanging wall, containing low-grade disseminated ore. Hybrid zones adjacent to the contacts with norite and olivine melanorite are well developed. Boulders and rafts of these rocks are locally abundant in the peridotite.

Regional setting

The whole Gabbro Akarem area has been subjected to post-emplacement, post-mineral faulting, and numerous faults disrupt the continuity of the peridotite (Fig. 3). The age of the Gabbro Akarem mafic body is almost certainly younger than the main episode of regional folding and low-grade metamorphism of the regional geosynclinal sediments. Emplacement occurred during the climax of the Pan-African orogeny, but predates the emplacement of older (G1) calc-alkaline granites and late-orogenic (G2) granites. Garson & Krs (1976) proposed that the emplacement of the mafic–ultramafic mass at Akarem took place along a deep-seated fracture zone, one of a series of ENE-trending zones controlling several geological features in the Eastern Desert. The reversely zoned structure in the Akarem complex is in accordance with the gradual deepening of the major fault-zone (Carter 1975). Rejuvenation along the Gabbro Akarem fracture zone is very pronounced, and the lineament has been intermittently active from the Proterozoic onward. The ENE trends of the transverse faults along which spreading in the present-day Red Sea was initiated appear to be controlled by this ancient deep fracture-zone (Krs 1977). The intrusive body itself has

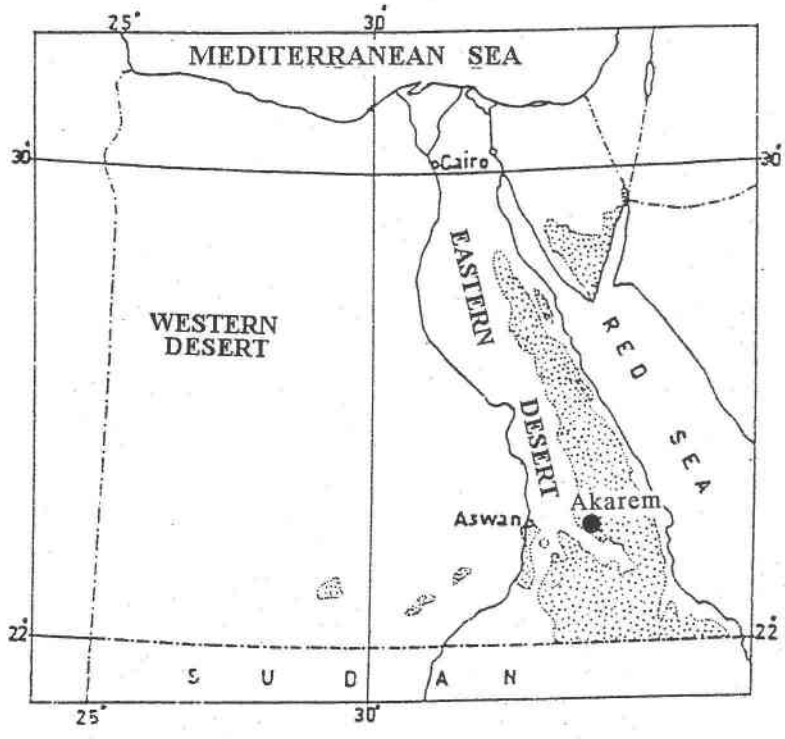

FIG. 1. Location map for the Gabbro Akarem intrusive complex, southeast Egypt.

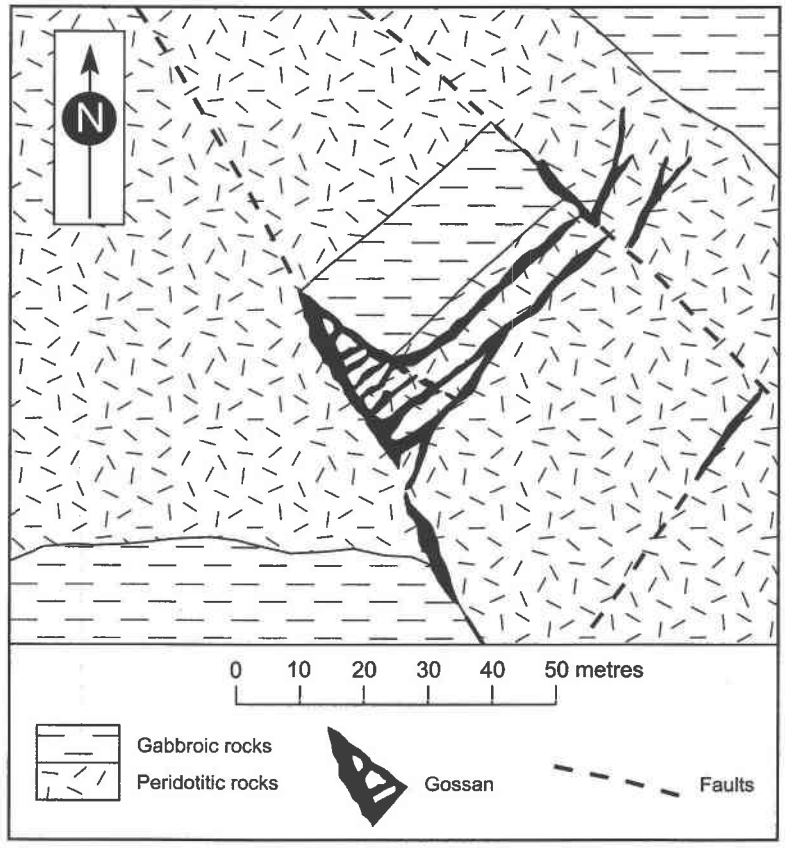

FIG. 2. Geological sketch-map of the southwestern gossan zone at Gabbro Akarem. After Bugrov & Shalaby (1973).

been described as "a unique on-shore analogue of ultrabasic intrusions in transverse tectonic structures which offset the Mid-Atlantic Ridge" (Carter *et al.* 1978).

The geophysical investigation by Guillon (1975) distinguished two peridotite phases, the more magnetic mineralized peridotite and a non-magnetic barren peridotite. The magnetic peridotite appears to form a pipe- or dyke-like body, steeply dipping in relation to the surrounding gneisses, and probably deep-rooted. The pipe is nearly vertical, with a rectangular plano-convex to elliptical horizontal section, and strikes 76°E. It attains a maximum length of 250 m and a width up to 80 m. It maintains a constant width and steep dip for at least the first 200 m below surface (Fig. 4).

The samples

The first geochemical surveys in Egypt were carried out in 1968 in the rocky Eastern Desert. The March 1972 discovery of Ni–Cu–Co sulfide mineralization in mafic–ultramafic rocks at Gabbro Akarem was a part of the UNDP Aswan project, 1968–1973 (Bugrov & Shalaby 1973, 1975). Carter (1975) inferred that to a depth of 130 m, there are 700,000 tonnes of mineralized peridotite grading 0.95% Cu + Ni. Samples for this study were collected from three drill holes (DH2, DH3 and DH7), whose locations are shown in Figure 4. Hole DH2 (inclined 60°) penetrated peridotite, pyroxenite and then gabbro and norite. Disseminated sulfides were encountered along the whole length, increasing with depth. The richest section is from 100.5 to 138.5 m, samples assaying 0.34–1.52 wt.% Cu (average 0.7 wt.%), 0.22–2.44 wt.% Ni (average 0.74 wt.%) and 0.018–0.136 wt.% Co (average 0.053 wt.%). The true thickness of this best-mineralized interval is estimated to be 13 m. Hole DH3 (vertical from the same collar as DH2) penetrated dense disseminated and massive sulfides at depths of 36–41.2 and 48–53 m. Hole DH7 revealed two mineralized zones in peridotites: (1) 53.5–67.0 m, with true width 10.7 m ("hanging-wall zone"), grading 0.46–1.18 wt.% Ni (average 0.75 wt.%) and 0.68–1.26 wt.% Cu (average 0.93 wt.%), and (2) 103–106 m, with true

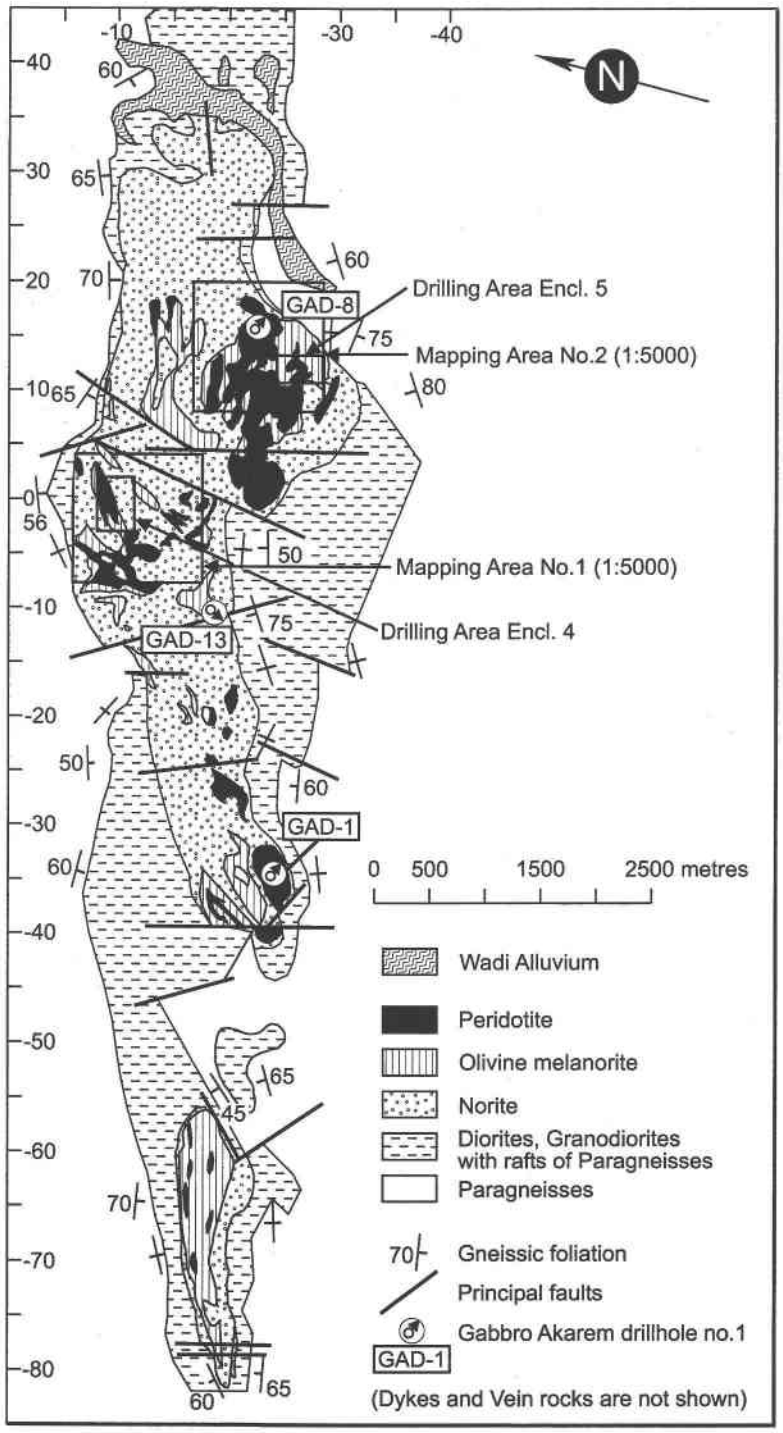

FIG. 3. Generalized geological map of the Gabbro Akarem area. After Carter (1975).

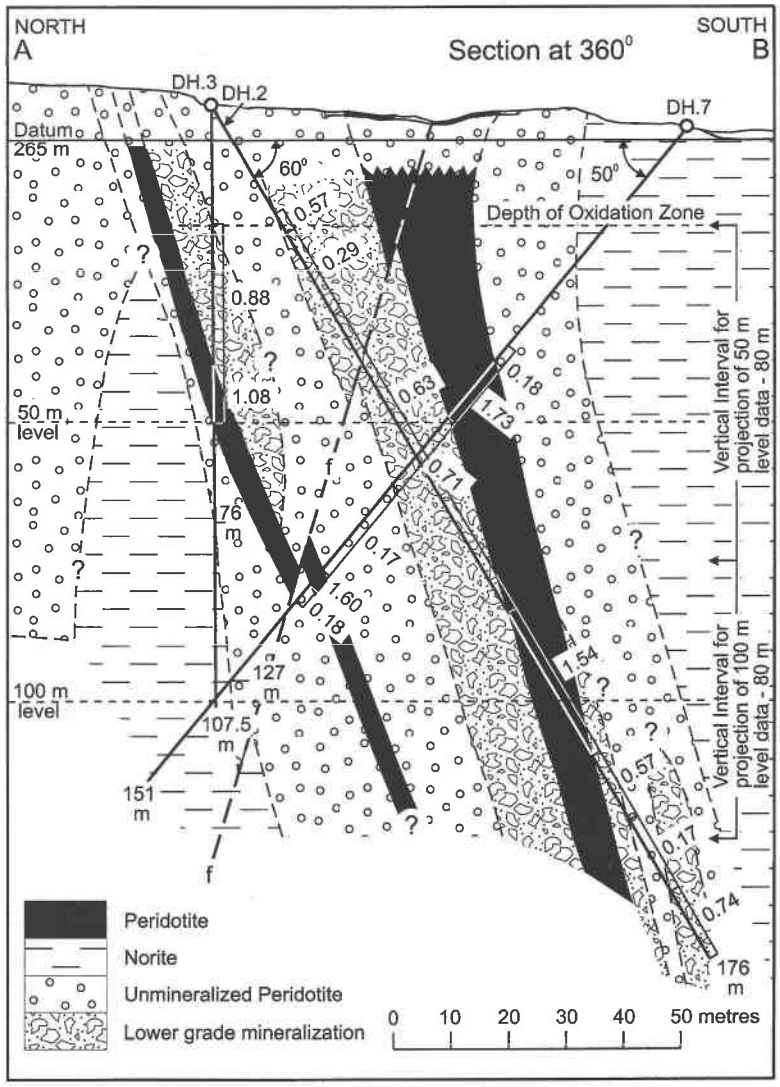

FIG. 4. Drillhole sections 2, 3 and 7. Gabbro Akarem, Area No. 1. After Carter (1975).

width 2.4 m (the "footwall zone"), with 0.4–1.19 wt.% Ni (average 0.85 wt.%) and 0.44–1.02 wt.% Cu (average 0.8 wt.%).

GENERAL FEATURES OF THE ORE

Essential ore minerals within the mineralized peridotite are pyrrhotite, pentlandite and chalcopyrite. There are three principal ore textures; network, disseminated and massive sulfides. In the first type, sulfides occur interstitially to cumulus olivine grains, forming an evenly distributed network. Disseminated ore usually occurs as discrete aggregates in interstitial voids of cumulus olivine, pyroxene and plagioclase. Massive ore occurs as veinlets and thin bands. Ore minerals are usually found interstitially to silicates, with little or no replacement except in zones of later shearing. The mineralized peridotite represents the residual sulfide-bearing fraction derived from a magnesian (>20% MgO) parental magma that experienced fractional crystallization and accumulation. Typical textures of sulfide-rich samples from the drill cores are shown in Figure 5.

The ore textures are consistent with the formation of immiscible sulfide–oxide droplets, plausibly concentrated by magmatic accumulation prior to emplacement, with further gravity settling during consolidation in the

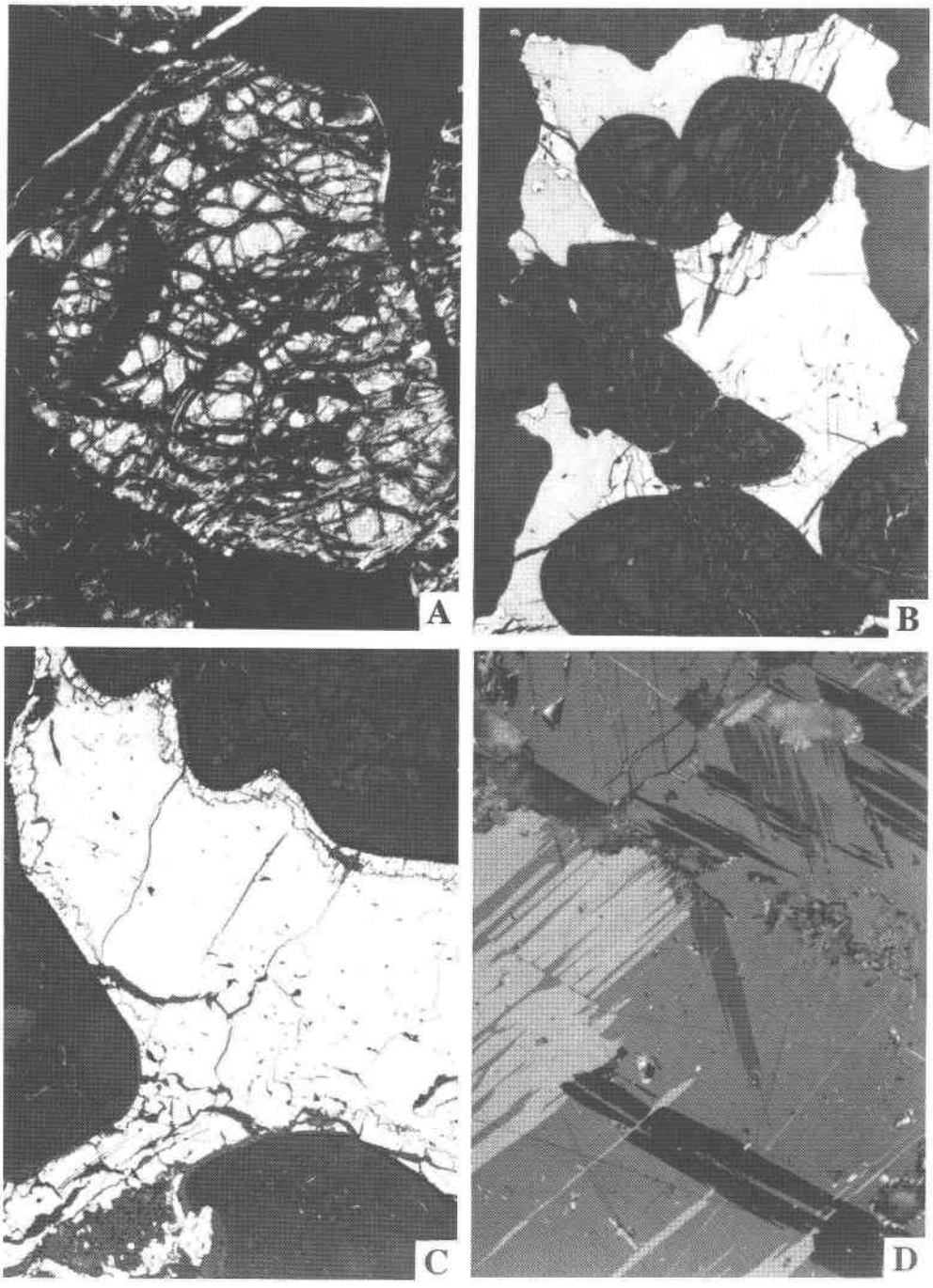

FIG. 5. Typical textures in sulfide-rich rocks from Gabbro Akarem. A. Partly serpentinized olivine in net-textured sulfides of peridotite from drill hole DH2. Cross-polarized light, long-axis field of view 2.8 mm. B. Sulfide-bearing serpentinized peridotite from DH2. Cumulus olivine, with wisps of secondary magnetite along serpentine veinlets, enveloped by net-textured sulfide (pyrrhotite with minor chalcopyrite and pale, granular pentlandite on margins). Plane-polarized light, 2.8 mm. C. Pyrrhotite and chalcopyrite, the former with a near-complete rim of granular pentlandite, in peridotite of DH7. Plane-polarized light, 1.4 mm. D. Exsolution lamellae of cubanite in chalcopyrite host in sulfide-bearing olivine websterite, DH2. Offset cross-polarized light, 0.7 mm.

TABLE 1. ELECTRON-MICROPROBE DATA FOR FORSTERITIC OLIVINE

SiO_2	MgO	FeO	MnO	CaO	NiO	Total	Fo%	Fa% 100 (Fe+Mn)/(Fe+Mn+Mg)
39.67	42.19	18.51	0.33	...	0.09	100.79	80.56	19.11	19.44
40.11	42.48	17.94	0.30	...	0.10	101.02	79.96	19.63	20.04
39.66	41.79	18.67	0.29	0.03	0.11	100.54	79.74	19.19	20.29
40.19	42.92	17.05	0.24	0.03	0.13	100.56	81.58	18.19	18.45
Average									
39.91	42.33	18.04	0.29	0.01	0.11	100.69	80.46	19.03	19.55

Cr not detected. Proportion of oxides in wt.%.

TABLE 2. ELECTRON-MICROPROBE DATA FOR PLAGIOCLASE

Na_2O	FeO	K_2O	SiO_2	CaO	Al_2O_3	TiO_2	Total	Ab %	Or%	An%	Total
5.94	0.08	0.19	56.95	9.29	28.08	0.01	100.54	58.55	0.67	40.76	99.98
7.21	0.14	0.26	59.18	7.13	25.84	...	99.76	63.62	1.49	34.77	99.88
6.68	0.13	0.12	57.89	8.35	26.99	0.03	100.19	52.99	1.14	45.86	99.99
Average											
6.60	0.12	0.19	58.01	8.26	26.98	0.01	100.16	58.39	1.10	40.46	99.95

Proportion of oxides in wt.%.

magma chamber. A diffusive process is suggested whereby the sulfide droplets moved outward to the margins of the ultramafic pipe and concentrated in zones such as the "footwall and hanging zones" noted in DH7. Some remobilization of sulfides along shear planes occurred at a later time. The common occurrence of carbonate veinlets and gypsum associated with the ore has been ascribed to local contamination by reaction with the host garnetiferous metasediments. The mineralized peridotite commonly contains calcite and dolomite, both interstitial to cumulus olivine. Wallrock assimilation and loss of heat at the contact could in principle engender sulfur saturation of the mafic magma (Irvine 1975) but, as will be seen later, our S/Se and $\delta^{34}S$ data do not offer clear support for extensive contamination. Carbonate is not uncommon in altered peridotites (*e.g.*, James & Hawke 1984). The mineralized peridotite displays an assemblage dominated by primary amphibole, phlogopite and plagioclase, together with olivine and pyroxene. Reaction between olivine and plagioclase formed spinel-bearing symplectites. Results of electron-microprobe analyses of olivine and feldspar in the peridotite are given in Tables 1–2. The olivine averages $Fo_{80.5}$ and is Ni-poor forsterite (1100 ppm NiO), the plagioclase averages $Ab_{58.4}An_{40.5}$ (andesine), and the hornblende shows negligible Cl and F contents.

A remobilization of the sulfide fraction is evident; sulfides invade structures made available by deformation in the rock-forming silicates, infiltrating favorable cleavage and fracture planes in the ferromagnesian grains and cementing the host crystals. Sulfide remobilization is commonly accompanied by deuteric alteration of the host rock. Hornblende, tremolite and chlorite are intimately intergrown with remobilized sulfide and envelop grains of relict serpentinized olivine.

Mineralogy and Paragenesis

Estimated modal proportions of some representative sulfide-bearing rocks and their mode-indicated names are given in Table 3. The ore mineralogy is dominated by the following species.

Pyrrhotite ($Fe_{1-x}S$) and *troilite* (FeS): three related sulfides are observed, hexagonal pyrrhotite, monoclinic pyrrhotite and troilite. Hexagonal pyrrhotite (~Fe_9S_{10}) occurs as medium to coarse grains interstitial to olivine or chromite; it shows signs of deformation and cracking. Grain size ranges from 2 × 1.5 mm to 6 mm. Pyrrhotite occurs in both disseminated and massive forms in mosaic aggregates. It also replaces silicates. Electron-microprobe analyses show that the metal content varies, with ~0.1 wt.% Co, 0.2% Cu, 0.2–0.6% Ni, with an average composition near ($Fe_{0.99}Co_{0.001}Ni_{0.005}Cu_{0.004}$)

TABLE 3. ESTIMATED MODAL MINERALOGY AND ROCK NAMES

Sample	Ol	Srp	Opx	Cpx	Hbl	Pl	Po	Pn	Ccp	Various	Suggested Rock Name
DH2-110-116	20	36	1	2	2	3	30	4	2	Chr, Mgt, Cub, Cb, Ap	Sulfide-bearing serpentinized peridotite
DH2-136-142	13	5	6	50	4	4	7	1	8	Chr, Cb 1, Cub 1, Chl, Tlc	Sulfidic olivine websterite
DH3-55-59	38	10	1	8	4	1	30	4	4	Chr, Cub, Cb	Sulfide-bearing serpentinized peridotite
DH7-53-59-A,B	50	1	4	28	8	Tr.	6	1	2	Chr, Mgt, Cb, Tlc	Sulfidic hbl–cpx peridotite
DH7-100-103	46	4	4	20	10	Tr.	10	4	2	Chr, Mgt, Cb	Sulfidic hbl–cpx peridotite

Visually estimated contents in area (volume) percent, or noted "Tr." for trace amounts (<<1%). The "various" minerals are trace (accessory) phases, unless otherwise noted. Symbols: Ap: apatite, Cb: carbonates, Ccp: chalcopyrite, Chl: chlorites, Chr: chromite, Cpx: clinopyroxene, Cub: cubanite, Hbl: hornblende, Mgt: magnetite, Ol: olivine, Opx: orthopyroxene, Pn: pentlandite, Pl: plagioclase, Po: pyrrhotite, Srp: serpentine.

$S_{1.05}$. Hexagonal pyrrhotite is replaced by oxides and hydroxides of Fe, which are readily observed as iron-stained hematite and goethite. Monoclinic pyrrhotite (~Fe_7S_8) is formed by replacement of hexagonal pyrrhotite under oxidizing conditions. It has a variable stoichiometry; its upper stability limit is at 254°C. The modification of hexagonal pyrrhotite is due to the loss of part of its Fe content. Troilite (FeS) occurs intimately intergrown with low-temperature hexagonal pyrrhotite. This nominally stoichiometric compound is stable below 140°C (Yund & Hall 1969). Electron-microprobe analyses indicate the composition $Fe_{1.01}Ni_{0.001}S_{1.05}$.

Pentlandite $(Fe,Ni)_9S_8$ occurs as a massive, coarse sulfide, as a rim around pyrrhotite, and as minute flames and exsolved lamellae inside pyrrhotite. Octahedral cleavage and fracturing are best developed in the coarse pentlandite, which is earlier than the exsolved flames. This latter generation contains less Co and Ni than the primary magmatic pentlandite. The following average compositions (wt.%) of the pentlandite habits were determined by electron microprobe: coarse to massive pentlandite: Cu 0.10%, Co 2.61%, Fe 35.86%, Ni 27.34%, S 32.86%; exsolution "flames" in pyrrhotite: Cu 0.09%, Co 1.97%, Fe 34.00%, Ni 30.13%, S 33.33%.

The Akarem pentlandite is characterized by a relatively high Co content. The observed Ni/Fe value lies between 0.69 and 1.23, and the S content is 32.4–34.4 wt.%. Pentlandite may contain reticular intergrowths of chalcopyrite and pyrrhotite. The average grain-size of the pentlandite ranges from 0.5 × 0.7 mm to 2.4 × 1.7 mm.

Chalcopyrite ($CuFeS_2$) occurs in three different textural forms: coarse granular aggregates, narrow rims or small individual grains at pyrrhotite margins, and minute inclusions in pyrrhotite and pentlandite. In some cases, chalcopyrite fills cracks and fractures cross-cutting olivine and pyroxene. Chalcopyrite contains abundant cubanite. Intergrowths of chalcopyrite with pyrrhotite, pentlandite and cubanite are common. Co and Ni contents are low. The mean grain-sizes in samples range from 400 × 40 μm to 1.7 × 0.8 mm.

Violarite ($FeNi_2S_4$) is mostly found as partial or complete pseudomorphs after pentlandite and pyrrhotite. Violarite invades pyrrhotite along cracks, and usually assumes a lamellar habit. It is formed through partial removal of Fe and enrichment of Ni and S (Graterol & Naldrett 1971). The released Fe is progressively oxidized to magnetite, and then goethite. Misra & Fleet (1973) noted that violarite forms easily from pentlandite at low temperature and is stable over a wide range of oxidizing conditions. The violarite at Akarem is relatively Fe-rich. Nickel *et al.* (1974) suggested that wherever pentlandite is altered to violarite, the coexisting pyrrhotite partially converts to violarite, but the replacement of pyrrhotite ceases once pentlandite is almost completely replaced by violarite.

Cubanite ($CuFe_2S_3$) is found associated with chalcopyrite as characteristic lamellae, as sharply bounded laths and as irregular granular aggregates. Cubanite separates from chalcopyrite at 250–300°C. The grain size ranges from 200 × 5 to 800 × 300 μm.

Millerite (NiS) is an uncommon fine- to medium-grained accessory at Akarem. A few anhedral grains are found intergrown with violarite, and it may replace pentlandite and pyrrhotite.

Mackinawite (FeS_{1-x}) is formed under reducing conditions, during partial serpentinization of the peridotite, where it replaces pentlandite and occasionally chalcopyrite; similar cases were reported by Genkin (1971) and Eckstrand (1975). It is found with troilite or with low-temperature pyrrhotite in a range of environments. Berner (1964) precipitated this phase from aqueous iron sulfide solutions between 20 and 95°C. The metal:sulfur ratio is slightly greater than unity, 1.04–1.07. The formula is usually written ($Fe_{1+x}S$). Taylor & Finger (1970) have shown that there is a deficiency of S rather than an excess of metal. It forms a network of worm-like microveinlets or minute aggregates in pentlandite and, less commonly, chalcopyrite.

Magnetite (Fe_3O_4) forms euhedral, rounded or even skeletal crystals. It may contain fine laminae of exsolved ulvöspinel or ilmenite. Alteration upon serpentinization includes some replacement of sulfides by magnetite (Hafez & Abdel-Kader 1982).

Chromite [$(Fe,Mg)Cr_2O_4$] occurs in minute rounded to subrounded grains usually associated with olivine.

Pyrite or marcasite or both (FeS_2) are secondary sulfides after pyrrhotite. Colloform masses with a bird's-eye texture are common where pyrite is found in association with goethite. Marcasite is metastable, and it readily converts into pyrite.

Mode of formation of pyrrhotite

Studies of the phase relations in the systems Cu–Fe–Ni–S and Fe–O–S have shown that the earliest-formed sulfide phase is a nickeliferous and cupriferous pyrrhotite (hexagonal phase) or monosulfide solid solution (*mss*). Hexagonal pyrrhotite will be exsolved in the temperature range 734–254°C. Removal of Fe from *mss* results in relative enrichment in S and thence the conversion of any hexagonal pyrrhotite to the monoclinic form. According to the Fe–S–O phase diagram of Kullerud (1957), nucleation of pyrite from S-saturated hexagonal pyrrhotite with the production of magnetite could start at temperatures as high as 675°C, and if oxygen is added to the system, S-enriched hexagonal pyrrhotite will convert to monoclinic pyrrhotite. The formation of monoclinic pyrrhotite starts at ~254°C. Monoclinic pyrrhotite and pyrite are stable over the range 254–75°C and are usually formed by progressive equilibration on cooling of high-temperature, S-saturated pyrrhotite. The metastable association of hexagonal and monoclinic pyrrhotite + pyrite commonly persists in natural ores. Exsolution of troilite from hexagonal pyrrhotite proceeds down to a very low tempera-

ture, <100°C (Garuti & Rinaldi 1986).

Mode of formation of pentlandite

According to Naldrett (1969), pentlandite may form by exsolution from a nickeliferous pyrrhotite by subsolidus equilibration on cooling of the original *mss* below ~615°C. A plot of the bulk composition of the Akarem mineralized peridotite on the Fe–Ni–S diagram shows that most of the samples fall within the *mss* field at 600°C, thus suggesting that pentlandite is mainly a result of exsolution. Misra & Fleet (1973) showed that Ni-rich pentlandite does not appear until the temperature has fallen well below 200°C, which is considerably lower than the temperature of formation of monoclinic pyrrhotite. Durazzo & Taylor (1982) noted that pentlandite is not exsolved in massive form but acquires this texture through growth and coarsening on cooling. The massive habit of pentlandite seems to indicate a higher temperature, whereas the exsolution of lamellar pentlandite mostly takes place at a lower temperature than the massive forms and marginal rims on earlier sulfide (Durazzo & Taylor 1982). Vaasjoki *et al.* (1974) determined that the thermal stability of pentlandite increases with the presence of Co in the structure, and thus upon cooling of magmatic sulfide ore, Co-rich pentlandite could crystallize at a higher temperature than the normal pentlandite. The estimated average Co content of Akarem pentlandite is 2.24 wt.%.

Mode of formation of chalcopyrite

Bulk analyses of the mineralized peridotite of Gabbro Akarem show that the sulfide fraction contains ~5 wt.% Cu, of which all could have been carried in solid solution in the original *mss* at the time of its crystallization (Yund & Kullerud 1966). It follows that the bulk of the observed chalcopyrite should have formed by subsolidus exsolution. On account of the modest bulk Cu content at Akarem, chalcopyrite must have exsolved below 450°C (Craig *et al.* 1967). The presence of mackinawite and cubanite lamellae in chalcopyrite indicates that the chalcopyrite precursor, an intermediate solid-solution (*iss*), exsolved from the *mss* at relatively high temperature and was rather Fe-rich. Pauly (1958) concluded that Cu-rich "chalco-pentlandite" exsolves from pyrrhotite at 850°C, then separates into pentlandite and chalcopyrite at 600°C. Ramdohr (1969) proposed that chalcopyrite formed by unmixing is rare, and confined to occurrences formed at exceptionally high temperatures. Naldrett (1979) attributed the occurrence of fine veinlets of sulfide amongst silicate minerals, particularly along fractures and cleavage planes, and the formation of symplectitic intergrowths, to small-scale remobilization of sulfides after exsolution from the original *mss* in response to tectonic stress and the action of deuteric or metamorphic fluids.

Late-Stage Processes

Rasmy (1982a) inferred that the low level of Zn involved in the mineralization, indicated by the almost complete absence of sphalerite, excludes late epigenetic hypotheses to explain the introduction of ore metals. In many mobilized ores, Cu may be selectively carried in solution by the circulating fluids after exsolving from the original *mss* below 450°C, or it may crystallize from a Cu-rich liquid at a temperature as high as 850°C. The temperature at Akarem must have been below the solidus of mafic silicates, but still high enough to allow pyroxene to be folded in a plastic manner, whereas the molten sulfide was free to move and to be squeezed into zones of lower pressure. This situation implies that the bulk of the silicate magma solidified before the onset of sulfide crystallization, which is consistent with the interstitial position of sulfides in undeformed samples.

The mobilization process seems to have occurred under conditions not far removed from the crystallization of the primary, magmatic sulfide. Mobilization would, however, cause fractionation of the sulfide melt. Thus a Cu-enriched residual liquid may account for the confinement of chalcopyrite to late-stage fissure-fillings in silicates. The textures of the mobilized ores provide evidence that mobilization occurred in response to deformation, not long after segregation from the silicate phase.

S/Se and $\delta^{34}S$ data constrain the origin of the S (Table 4). Four aliquots of one sample from each of the three drill holes returned very consistent results, with a mean S:Se ratio of 4300 ± 1200 ($2\sigma_{n-1}$), range 3900–5150 (mean Se/S = 233 × 10^{-6}). Eight aliquots of these same samples were analyzed for their S isotopes, with a tight cluster of $\delta^{34}S$ = +1.0 to 1.3‰ (extreme range +0.7 to 1.5‰). These findings are consistent with a magmatic, mantle signature, although in the absence of data for the wallrocks to the conduit(s) of Akarem magmas, it is impossible to rule out a degree of crustal contamination (*cf.* Eckstrand *et al.* 1989, Peltonen 1995, Ripley 1990).

Concentration of PGE and Gold

In situ analyses of selected sulfide minerals from drill holes 2, 3 and 7 were made by Accelerator Mass Spectrometry (AMS). In addition, representative (~20 g) aliquots were analyzed for bulk PGE and Au using ICP–MS and INAA methods, in each case with a fire-assay preconcentration step. Details of the AMS method, and its relationship to the family of more-familiar microprobe techniques, are reviewed (Wilson *et al.* 1995, 1997, Wilson 1998) and described elsewhere (Wilson *et al.* 1998).

The distribution of PGE and Au in individual minerals is given in Table 5, and bulk values and estimated levels in 100% sulfide are shown in Tables 6–7. Bulk

TABLE 4. S/Se AND $\delta^{34}S$ DATA FOR SULFIDE-RICH ROCKS

A. The Se/S values

MDL	S (wt.%) 0.01	Se (ppm) 0.1	Rounded S:Se ratio
Samples			
DH2 – 1	28.9	59.6	4850
DH2 – duplicate	28.6	55.5	5150
DH2 – mean	28.7	57.5	5000
DH3	10.3	26.4	3900
DH7	11.8	29.4	4010
Mean			4300 ± 1200 ($2\sigma_{n-1}$)
Range ± $2\sigma_{n-1}$			3100–5520

B. The S isotope data

Samples	Weight (g)	S (wt.%)	$\delta^{34}S$ (‰)
DH2	0.357	28.30	1.11
	0.312	29.45	1.20
Mean		28.87	1.16
DH3	0.572	11.01	1.48
	0.573	9.78	0.99
	0.526	10.44	0.67
Mean		10.41	1.05
DH7	0.634	12.20	1.45
	0.599	11.64	1.16
	0.616	11.79	1.34
Mean		11.88	1.32

MDL: minimum detection limit.

TABLE 5. AMS DATA ON PRECIOUS METALS IN AKAREM SULFIDES

Sample	Point	Ir	Rh	Pt	Pd	Au
E (DH7-53-59)						
E, Po - M	3	63	96	1.4	450	25.0 (V)
E, Po	4	53	47	0.8	4.6	2.9
						3.3
E, Po	5	68	77	1.5	47.0 (V)	4.2
						4.3
E, Po	6	64	115	1.8	105.0 (V)	2.4
						3.4
Mean		62.0±6	83.8±29	1.4±0.4		3.4±0.7
B (DH2-110-116)						
B2, Ccp - M	9	0.7	6.7	n.d.	500	1.8
						1.7
B2, Po - M	10	0.2	1.9	n.d.	50	2.0
						1.6
B2, Pn - M	11	0.2	0.25	1.0	45	2.9
						2.8
F (DH2-116-122)						
F, Po	12	40	28	0.9	9.8	4.8 (V)
F, Po	13	27.5	26	1.0	2.7	3.3
						1.8
F, Po	14	96	23	1.0	7.1	3.0
						2.1
Mean		54.5±36	25.7±2.5	0.95±0.05	6.5±3.6	2.6±1.4
D (DH3-55-59)						
D, Ccp - M	16	2.8	40	1.1	80	8.2
						4.5
D, Po - M	17	3.7	48	0.9	770	2.8
						2.2
D, Pn - M	18	4.9	17	0.5	1030	8.4 (V)
Cu	15	4.5	n.d.	2.0	n.d.	35.0
						32.3
SARM 7	1,2,7,8	113	366	5696	2330	472
MDL		0.17	0.24	0.4	1.8	0.02

All values in ppb by weight. "n.d.": not detected, below quoted minimum detection limit (MDL) for each element. "M" denotes a mixture of the predominant phase with traces of other sulfides. The key or only mineral in each point is listed: pyrrhotite (Po), chalcopyrite (Ccp) and pentlandite (Pn). The SARM 7 values are the estimated values for the reference material, a NiS bead with 1.523 times the accepted metal contents of the parent geostandard. Where major variation is seen, more than a factor of 3–5, or where there is a strong trend in values with time, indicative of the presence of grain boundaries or mineral inclusions, the data are labeled V (variable), *e.g.*, Au in points 3 and 18 varied from 7 to 100 and 1 to 40 ppb in single 10-s counts. Gold data are the means of each pair of 10-s counts on each point. The Au mean of sample E is calculated from points 4–6 alone, that of F from points 13–14. Pt is presented as one mean of three 100-s counts on each point, and the other PGE data are condensed in similar fashion. MDLs for Ir, Rh and Pd may appear low (relative to Au and Pt) in light of past work. In this instance, however, these three elements were detected as q = +5 ions, Au and Pt as q = +6, which are generated at lower efficiency with 2 MV terminal voltage.

compositions for the AMS-analyzed samples are shown in Table 8. Coarse-grained sulfides, as crystals up to 3 mm across, were selected for the *in situ* analyses. The mean results of bulk-rock and single-crystal analyses are grouped in Table 9. The wide variation in the results are primarily attributed to the inhomogeneous distribution of the PGE in a single grain. Estimated partition coefficients for the different PGE and Au are shown in Table 10.

Pyrrhotite

Gold and all PGE except Os (not sought) and Ru were detected in pyrrhotite from the three drill holes at different depths in the mineralized peridotite (Table 5). Nine grains of pyrrhotite were analyzed, both the footwall and hanging wall being sampled. The variation in the level of the PGE among the different grains suggests inhomogeneous distribution of these elements in pyrrhotite. Pt, Pd and Au in pyrrhotite are very much lower than in the bulk sulfide-rich rocks, whereas the Ir and Rh contents of pyrrhotite exceed bulk levels.

Pentlandite

Pentlandite accommodates significant amounts of Pd, up to a minimum of 1 ppm. Although unremarkable compared to other examples of pentlandite reported in the literature, this is up to five times the bulk values. All other PGE and Au are very much lower than their level in the bulk rocks.

Chalcopyrite

The amount of Pd in chalcopyrite varies from 50 to 500 ppb, Rh ranges from 0.25 to 117 ppb, Ir from 0.2 to 4.9 ppb, Pt from 0.1 to 0.5 ppb, and Au from 2.8 to 8.4 ppb. All the average values are much lower than those of the bulk sulfide ore. Mean contents in chalcopyrite

TABLE 6. CONCENTRATIONS OF PGE AND BASE METALS IN GABBRO AKAREM PERIDOTITIC ORE

Sample	S%	Co%	Ni%	Cu%	Os	Ir	Ru	Rh	Pt	Pd	Au
AK1	13.7	0.10	1.5	0.71	7.91	11.4	16.3	27.2	60.1	105	53.5
AK2	11.4	0.08	1.29	0.4	3.21	6.45	12.5	15.2	99.2	82.6	33.0
AK3	5.19	0.03	0.52	1.68	1.0	0.98	1.0	2.09	82.4	47.6	120
AK4	1.43	0.02	0.21	0.22	1.0	0.29	1.0	1.0	58.3	1.0	42.6
AK5	2.3	0.02	0.26	0.15	1.0	1.03	1.0	3.39	30.8	1.0	20.8
AK6	4.14	0.03	0.41	0.96	1.0	2.15	1.0	4.5	31.1	1.0	44.6
AK7	6.67	0.05	0.71	0.58	1.35	1.37	4.79	3.65	326	71.5	34.1
AK8	3.4	0.03	0.33	1.04	1.0	1.05	1.0	1.69	139	1.0	550

Concentrations of S, Co, Ni, Cu in wt.%, and of PGE and Au in ppb. Provenance of samples: AK1: DH2, 95–122 m. AK2: DH2, 122–136 m. AK3: DH2, 136–142 m. AK4: DH3, 41–55 m. AK5: DH3, 55–59 m. AK6: DH7, 53–67 m. AK7: DH7, 97–103 m. AK8: DH7, 129–130 m. Analysis by NiS fire-assay with INAA finish at the Slowpoke reactor facility, University of Toronto.

TABLE 7. CALCULATED METAL VALUES IN 100% SULFIDE, GABBRO AKAREM

Sample	S%	Ni%	Cu%	Os	Ir	Ru	Rh	Pt	Pd	Au
AK1	38.8	4.24	2.01	22.4	32.4	46.0	76.9	170	298	151
AK2	38.8	4.39	1.36	10.9	22.0	42.6	51.9	338	281	112
AK3	37.5	3.75	12.13	-	7.1	-	15.1	595	344	866
AK4	38.1	5.59	5.86	-	7.8	-	-	1554	-	1135
AK5	38.7	4.37	2.35	-	17.3	-	57.1	519	-	349
AK6	37.9	3.75	6.79	-	19.7	-	38.9	285	-	409
AK7	38.6	4.11	3.36	6.6	7.9	27.8	21.1	1888	414	197
AK8	37.6	3.62	11.39	-	11.5	-	18.5	1525	-	6030

Concentrations of S, Co, Ni, Cu in wt.%, and of PGE and Au in ppb. Provenance of samples as in Table 6. The eight samples average an estimated 4.23% Ni and 5.65% Cu in 100% sulfide.

TABLE 8. AKAREM AMS-ANALYZED SUITE: WHOLE-ROCK CONCENTRATION OF PRECIOUS METALS

Sample	Ir	Rh	Pt	Pd	Au	ΣPGE+Au	Pd/Ir
A (DH2-122-128)	9.8	40.4	34.9	376.1	247	708	38
B (DH2-110-116)	5.5	41.8	122.4	151.9	64	386	28
C (DH2-136-142)	-	2.5	324.9	184.3	166	679	?
D (DH3-55-59)	3.0	22.4	20.5	111.4	1080	1237	37
E (DH7-53-59)	-	-	16.8	51.3	67	137	?

All results in ppb, Pb fire-assay and ICP–MS finish, at Activation Laboratories, Ancaster, Ontario. "-": not detected, set to nominal 1 ppb in the log-normalized plot, Figure 6. Rh and Ir are partial extractions, and thus minimum values.

TABLE 9. AVERAGE PGE AND Au VALUES, GABBRO AKAREM SUITE

Suite	S%	Ni%	Cu%	Os	Ir	Ru	Rh	Pt	Pd	Au
1	6.04	0.65	0.72	1.7	3.1	4.2	7.2	103	34	112
2	38.2	4.22	5.66	5.0	15.8	14.6	35.0	867	167	1131
3					3.7		21.5	104	175	325
4					58		54.8	1.08	115	2.4
5					2.5		8.6	0.75	537	4.7
6					1.7		23.3	0.65	290	4.0

Concentrations of S and base metals in weight percent, precious metals in ppb. 1. Mean measured content of S, Ni, Cu, PGE and Au in Gabbro Akarem rocks (Table 6). 2. Average estimated composition of 100% sulfide in mineralized peridotites (Table 7). 3. Mean bulk concentration of PGE and Au in samples selected for AMS analysis (Table 8). 4. Average of PGE and Au in pyrrhotite (AMS data, Table 5). In the instances of Ir and Rh in pyrrhotite, the average values for two groups of coarse grains are used to derive a mean. 5. Average of PGE and Au in pentlandite (AMS data). 6. Average of PGE and Au in chalcopyrite (AMS data).

TABLE 10. PARTITIONING OF PGE BETWEEN MSS AND SULFIDE LIQUID

Metal	Pyrrhotite	Pentlandite	Chalcopyrite
Ir	3.7	0.16	0.11
Rh	1.6	0.25	0.66
Pt	1.2×10^{-3}	0.9×10^{-3}	0.8×10^{-3}
Pd	0.7	3.2	1.7
Au	2.1×10^{-3}	4.1×10^{-3}	3.6×10^{-3}

Estimates for the partition coefficient $X_{[mineral]} / X_{[mss]}$ calculated from the values in Table 9.

are: 280 ppb Pd, 23.3 ppb Rh, 1.7 ppb Ir, 0.5 ppb Pt, and <5 ppb Au.

Crushed aliquots of the sulfide-rich rocks were analyzed for Fe, Ni, Cu, Co and S, and the calculated results were compared with the modal estimate of the respective sulfide minerals assuming that the ore is formed of pyrrhotite, pentlandite and chalcopyrite. The proportions (in wt.%) of pyrrhotite : pentlandite : chalcopyrite are estimated to be 73.0 : 10.2 : 16.8, respectively. With the average values for pyrrhotite and for the bulk sulfide ore, a mass-balance calculation indicates that almost 100% of the Rh and Ir and 68% of the Pd occur in pyrrhotite. Only 0.1% of the bulk Pt and 0.2% of bulk Au are accounted for by the pyrrhotite. Because the analyzed grains of pyrrhotite are free of visible inclusions of PGM (by ore microscopy and casual SEM survey, thus ruling out inclusions >1 μm), it is likely that these elements are essentially absent from pyrrhotite, not occurring in solid solution, nor as submicroscopic inclusions, nor as atomic clusters, as may be the case for Au in pyrite, for example (Bakken *et al.* 1989).

In contrast, pentlandite and chalcopyrite host significant levels of Pd. Whereas 25% of Rh, 0.4% of Au, 0.1% of Pt and 16% of the Ir in the bulk ore are accounted for by pentlandite, about 66% of the bulk Rh and only 0.4% of Au, 0.1% of Pt and 16% of the Ir are hosted by chalcopyrite. Osmium was not sought, and Ru was not detected in the sulfides during routine 100-s counts.

Concentrations of Pt, Au, Ir and Rh are very low in the primary sulfides in comparison with their whole-rock contents. The majority of the Pt and Au must occur as discrete grains. Native gold is an accessory phase,

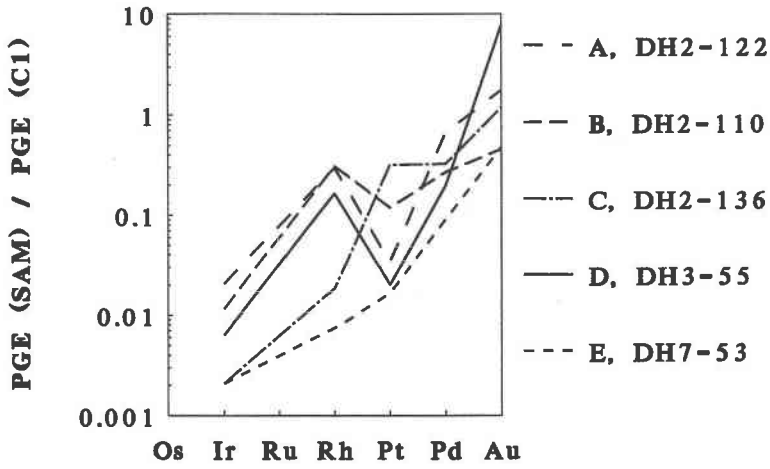

FIG. 6. Whole-rock PGE analyses for Akarem mineralization. Fire-assay – ICP–MS data from Activation Laboratories, Ancaster, Ontario, on ~20-g aliquots. Concentrations in the samples are normalized to a mean value for C1 carbonaceous chondrite meteorites.

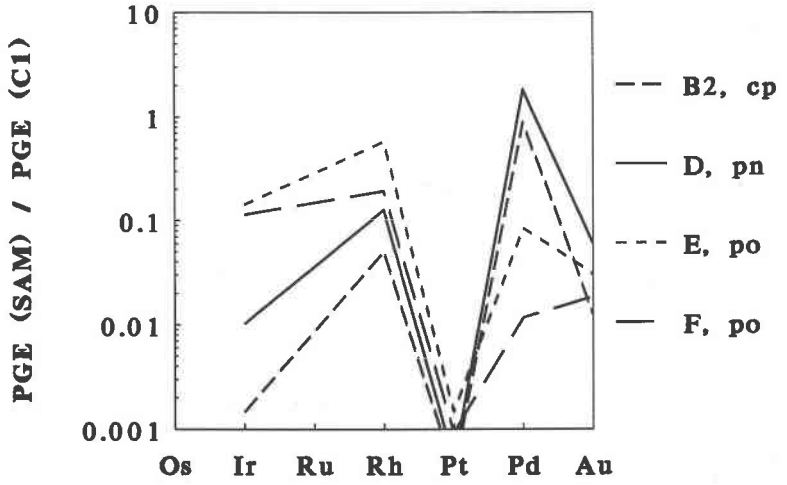

FIG. 7. PGE patterns in Akarem mineral grains. The *in situ* PGE concentrations were obtained by accelerator mass spectrometry for sulfide-rich aggregates in B and D and pyrrhotite grains in samples E and F. Sample B2: sulfide-rich area rich in chalcopyrite, with Pt below the minimum detection-limit (MDL). Sample D: pentlandite-rich sulfide aggregate. Sample E: coarse pyrrhotite. Sample F: mean of three points on coarse pyrrhotite (two points only for Au).

and its grain size is 18–35 μm. Electron-microprobe analyses gave a compositional range for gold grains with fineness 750–900, varying from ~90% Au and 10% Ag to 75% Au, 20% Ag and 5% Bi. Figures 6 and 7 show the PGE patterns of the whole-rock samples and individual grains analyzed *in situ*. More than 98% of the Au as well as most of the Pt must occur in discrete grains, not in sulfides.

Some Pd occurs in discrete PGM. Helmy *et al.* (1998) mentioned the detection of three tellurides, including two PGM at Gabbro Akarem: melonite ($NiTe_2$), merenskyite (PdTe) and michenerite (PdBiTe). No Pt-dominant PGM have been reported to date, but the AMS data suggest the probable existence of at least one such carrier as a rare accessory phase.

Partitioning of PGE between mss and sulfide liquid

If the average Pt content in pyrrhotite (1.08 ppb) is assumed to be that of the original *mss* that crystallized from the parental sulfide liquid, the partition coefficient ($X_{[mineral]}$ / $X_{[mss]}$) would have been ~1.2×10^{-3}. Makovicky *et al.* (1986) found that considerable amounts of PGE and Au enter *mss* at higher temperatures and exsolve at a lower temperature. On the other hand, that amount of Pt may not represent its concentration in *mss* at the time of crystallization, and therefore this partition coefficient is the minimum value. The partition coefficients of the PGE between *mss* and sulfide liquid are estimated from the concentration of the element in the mineral divided by its bulk concentration in the calculated 100% sulfide fraction. Table 10 gives *D* values for PGE and Au in the three analyzed sulfides.

Genetic Implications of PGE and Au in the Akarem Intrusion

Fe-rich *mss* is the first phase to crystallize from an Fe–Ni–Cu sulfide liquid (Kullerud 1967, Craig & Scott 1974), and it should behave like pyrrhotite in the system Ni–Fe. The total PGE and Au content of the Akarem mineralized peridotite is generally ≤3 ppm, whereas the abundant sulfides in the suite may average ~27% by volume, and locally account for a high proportion of the mass of the rock (Tables 8, 9). Thus there is ample *mss* to dissolve all the PGE. However, the amount of PGE that can be dissolved in *mss* will depend on the partitioning of these elements between *mss* and sulfide liquid. It is possible that all the PGE partitioned into *mss* and were in solid solution at high temperature.

Makovicky *et al.* (1986) studied the solubility of PGE in base-metal sulfides in systems of the form Fe–PGE–S and Cu–Fe–PGE. They found that at 900°C and high $f(S_2)$, pyrrhotite can in principle dissolve up to 11 wt.% Pd, 1.2 wt.% Pt, 3.6 wt.% Ru and 44 wt.% Rh. They also found that at 500°C, pyrrhotite dissolves only 0.4 wt.% Pd, an undetectable amount of Pt and Ru, and 6.7 wt.% Rh, whereas pentlandite can accommodate up to 12.5 wt.% Pd, 12.4 wt.% Rh, 12.9 wt.% Ru, but (relatively speaking) minimal Pt. Their experimental results show the relative importance of pyrrhotite and pentlandite in concentrating PGE and the effect of temperature on PGE solubility in sulfides. Their experiments show that pentlandite is much richer in Pd and Ru, but not in Rh, than the coexisting pyrrhotite. The Pd contents of the Akarem pentlandite may not be directly related to its concentration in the bulk sample, but to the sulfide fraction within the sample. Pentlandite at Akarem is the product of exsolution due to the subsequent cooling of *mss*; therefore Pd enters pentlandite, leading to its depletion in pyrrhotite. The preference of Pd in sulfides of Akarem is in the order pentlandite > pyrrhotite > chalcopyrite.

The wide variation of Pd within pentlandite in the analyzed grains suggests that diffusion of Pd through the *mss* was not sufficiently rapid to permit equilibrium to be attained during exsolution of pentlandite. The higher Pd content hosted in pentlandite agrees well with the data of Cabri & Laflamme (1976) on Sudbury, Keays *et al.* (1981) on Kambalda, and Barnes & Naldrett (1985) on Stillwater ores.

Makovicky *et al.* (1986) found that at 900°C, Pt is distributed between coexisting pyrrhotite and sulfide liquid, but favors the sulfide liquid (6–15 wt.%) over the pyrrhotite (~1 wt.%). In other words, Pt is incompatible in *mss* relative to the sulfide liquid, and therefore pentlandite exsolved from *mss* will be depleted in Pt. Thus most of the Pt will remain in the sulfide liquid and form independent PGM at a late stage of crystallization.

Li *et al.* (1993) reported relatively higher concentrations of Ir, Ru and Os in pyrrhotite, which represents the product of low-temperature equilibration of the early-crystallizing *mss* at the Strathcona mine in Sudbury. Naldrett *et al.* (1992a, b) noted that Ir partitioned strongly (D = 3) into *mss* that crystallized from the parental sulfide liquid of the ores at Noril'sk, Siberia. The high content of Ir in the Akarem pyrrhotite relative to bulk samples thus may represent low-temperature equilibration of the early-crystallizing *mss*.

It is known that *mss* started to form at Akarem at a high temperature, >750°C, from a sulfide melt in equilibrium with silicate melt. The $f(S_2)$ of a sulfide melt – silicate melt mixture is defined by the activity of FeO in silicate melt and the prevailing $f(O_2)$. Shima & Naldrett (1975) determined $f(S_2)$ values for a sulfide melt starting to crystallize at 1150°C. The relatively low $f(S_2)$ in the sulfide melt of Akarem can be inferred from (1) the metal-rich nature of the pyrrhotite, (2) the absence of primary pyrite, and (3) the common occurrence of cubanite and mackinawite.

This interpretation is consistent with either conditions of sulfur saturation in the mafic magma or an (expected) addition of sulfur from an external source. We believe that saturation may have occurred at depth and that only a small amount of sulfides were transported to the zone sampled by drilling (depth below the surface <200 m). Magnetite is relatively rare among the primary ore minerals, indicating low $f(O_2)$. Diffusion of oxygen toward the host silicate magma could be responsible for the reduction of the sulfide melt. Naldrett (1969) emphasized that when the sulfide melt occurs as relatively small dispersed particles in the host magma, that melt's $f(O_2)$ is buffered by the surrounding silicate. Oxygen diffusion took place at an early stage of differentiation, as suggested by the common presence of troilite in olivine-bearing rocks. Troilite also is common in carbonate-bearing zones, perhaps reflecting reaction with the metasediments. A high activity of CO_2 in the mafic magma can constrain the $f(O_2)$ to such an extent that very low values are sufficient to nucleate an immiscible sulfide melt having a low sulfur:metal ratio (Buchanan & Nolan 1979).

Oxidation of the immiscible sulfide melt is indicated where the sulfur:metal ratio is higher [*i.e.*, at higher $f(S_2)$], and this is evident where hydrous alteration of pyroxene to amphibole and the corona textures of olivine, pyroxene, plagioclase and amphibole are observed. The Akarem sulfides were partially remobilized during the deuteric–hydrothermal phase or later, in a low-grade metamorphic stage. Sulfide segregation was coeval with crystallization of hydrous phases, mostly hornblende.

These conditions support the assumption that the immiscible sulfide melt was probably oxidized, with abundant primary magnetite. Widespread alteration of ferromagnesian silicates provides evidence for fluid infiltration along microfractures, and these fluids were probably active over a wide range in temperature. These fluids provided a suitable medium for transport and deposition of sulfides and associated precious metals. The mineralogy implies an extended phase of deuteric alteration involving abundant sulfide and amphibole. A limited role is left for metal mobilization during post-crystallization metamorphism and the partial serpentinization of olivine.

Conclusions

In conclusion, with the primary sulfides emplaced as an immiscible melt, the mineral paragenesis is considered to be as follows:

1. The early-crystallized sulfide was dominated by a homogeneous Fe–Ni–Cu–Co–S *mss*.

2. The sulfide assemblage formed entirely by subsolidus exsolution from *mss* upon cooling.

3. Hexagonal metal-rich pyrrhotite is the first primary ore mineral to have crystallized in the paragenetic sequence, above 750°C, and at 254°C hexagonal pyrrhotite was converted to monoclinic pyrrhotite by Fe diffusion to form magnetite and pyrite.

4. Exsolution of pentlandite started in the range 500–300°C and continued down to <100°C. The early exsolved pentlandite is usually Fe-rich and crystallized in a massive form, whereas at lower temperature, a higher-Ni pentlandite crystallized.

5. A similar pathway applies for formation of chalcopyrite–cubanite. The exsolution texture of the Cu sulfides suggests that they originally crystallized as intermediate solid-solution (*iss*) from Cu-rich sulfide liquid. They then exsolved from each other during cooling, as inferred from the phase diagram for the system Fe–Cu–S.

6. By continuous cooling to very low temperature, <100°C, troilite exsolved from the metal-rich hexagonal pyrrhotite.

7. Small-scale remobilization of sulfide and contained metals took place under stress in the presence of a hydrous phase. The role of host-rock assimilation appears minimal from our modest sampling of drill core, neither S:Se ratios nor $\delta^{34}S$ supporting substantial contamination of a primitive parental magma by crustal material. Although oxidation in CO_2-rich conditions may play a role in sulfide segregation, the observed carbonate is probably too late in the paragenesis to have played this role.

The Gabbro Akarem complex has an area of almost 11 km^2, of which nearly one-third is peridotite. The combined tenor of PGE and Au is of potential economic interest, reaching ~3 ppm. The common base-metal sulfides can account for much of Pd, Rh and Ir in the bulk samples of the ore, whereas we contend that most of the Au and Pt is present as discrete phases, occurring only at low levels (1–10 ppb or less) within the host sulfides themselves. Pd is present especially in pentlandite, with >90% of the Ir and Rh located in pyrrhotite. The distribution of the PGE suggests that the precious metals are closely related to sulfide-rich zones and intimately connected with the processes of formation of the sulfides and the conditions prevailing during the exsolution of these sulfides from the *mss*.

Acknowledgements

Some drill-core samples were provided by the Geological Survey of Egypt. A travel grant for the first author's work in Canada was funded by the Egyptian Ministry of Higher Education. Xiao-Lei Zhao tuned and programmed the AMS system at IsoTrace for the *in situ* measurements of PGE and Au concentration at IsoTrace. The Se and S contents of the sulfides were measured by XRAL Laboratories, Don Mills, and the S isotope data were supplied by the Environmental Isotope Laboratory, University of Waterloo. Whole-rock data (Table 6) were obtained from the Department of Geology, University of Toronto, courtesy of M. Asif and A.J. Naldrett. Bulk analyses by ICP–MS (Table 8) were conducted by Activation Laboratories of Ancaster, Ontario. George Taylor and Shawn McConville of the University of Toronto prepared the polished samples, and Claudio Cermignani facilitated the electron-microprobe analyses. Karyn Gorra prepared GCW's photomicrographs, Subhash Shanbhag redrafted Figures 2–4, and Giovanni di Prisco improved the French translation. The paper benefitted from perceptive reviews by B.M. Bakken and J.R. Craig.

References

Bakken, B.M., Hochella, M.F., Jr., Marshall, A.F. & Turner, A.M. (1989): High-resolution microscopy of gold in unoxidized ore from the Carlin mine, Nevada. *Econ. Geol.* **84**, 171-179.

Barnes, S.J. & Naldrett, A.J. (1985): Geochemistry of the J–M (Howland) Reef of the Stillwater complex, Minneapolis Adit area. I. Sulfide chemistry and sulfide–olivine equilibrium. *Econ. Geol.* **80**, 627-645.

Berner, R.A. (1964): Iron sulfides formed from aqueous solution at low temperatures and atmospheric pressure. *J. Geol.* **72**, 293-306.

BISHADY, A.M., SHALABY, I.M. & DIAB, M.B. (1991): Contribution to the petrology and geochemistry of Akarem complex rocks, south Eastern Desert, Egypt. *Sci. J. Fac. Sci. Menaufia Univ.*, 335-370.

BUCHANAN, D.L. & NOLAN, J. (1979): Solubility of sulfur and sulfide immiscibility in synthetic tholeiitic melts and their relevance to Bushveld-complex rocks. *Can. Mineral.* **17**, 483-494.

BUGROV, V.A. & SHALABY, I.M. (1973): First discovery of Cu–Ni sulfide mineralization in gabbro–peridotitic rocks in Eastern Desert of Egypt. *Geol. Surv. Egypt Annals* **3**, 177-183.

_____ & _____ (1975): Geochemical prospecting in the Eastern Desert of Egypt. *In* Geochemical Exploration 1974 (I.L. Elliott & W.K. Fletcher, eds.), Elsevier, Amsterdam, The Netherlands (523-530).

CABRI, L.J. & LAFLAMME, J.H.G. (1976): The mineralogy of the platinum-group elements from some copper–nickel deposits of the Sudbury area, Ontario. *Econ. Geol.* **71**, 1159-1195.

CARTER, G.S., ed. (1975): Final report on the investigation of copper–nickel sulfide mineralization at Gabbro Akarem. *Aswan Mineral Survey Project, Internal Report, Geol. Surv. Egypt.*

_____, GARSON, M.S., RASMY, A. & SIMPSON, P.R. (1978): A Proterozoic basic/ultrabasic intrusion in a transverse zone at Gabbro Akarem in the Eastern Desert of Egypt. *Precambrian Res.* **6**, A10.

CRAIG, J.R., NALDRETT, A.J. & KULLERUD, G. (1967): Succession of mineral assemblages in pyrrhotite-rich Ni–Cu ores. *Carnegie Inst. Wash., Year Book* **67**, 431-434.

_____ & SCOTT, S.D. (1974): Sulfide phase equilibria. *In* Sulfide Mineralogy (P.H. Ribbe, ed.). *Mineral. Soc. Am., Short Course Notes* **1**, CS 1-110.

DURAZZO, A. & TAYLOR, L.A. (1982): Exsolution in mss-pentlandite system: textural and genetic implications for Ni-sulfide ores. *Mineral. Deposita* **17**, 313-332.

ECKSTRAND, O.R. (1975): The Dumont serpentinite: a model for control of nickeliferous opaque mineral assemblages by alteration reactions in ultramafic rocks. *Econ. Geol.* **70**, 183-201.

_____, GRINENKO, L.N., KROUSE, H.R., PAKTUNC, A.D., SCHWANN, P.L. & SCOATES, R.F.J. (1989): Preliminary data on sulphur isotopes and Se/S ratios, and the source of sulphur in magmatic sulphides from the Fox River sill, Molson Dykes and Thompson nickel deposits, northern Manitoba. *Geol. Surv. Can., Pap.* **89-1C**, 235-242.

EL MAHALAWY, M.M. & HELMY, H.A. (1997): Petrology, geochemistry and petrogenesis of the Gabbro Akarem mafic–ultramafic intrusion, south Eastern Desert, Egypt. *Third Conf. on Geochemistry (Alexandria, Egypt)* **2**, 67-84.

EL SIDECK, S. & EL GORESY, A. (1996): Phase relation of sulfide-minerals in Akarem area and platinum-group minerals in chromites from Abu Seifein chromitite. *Geol. Surv. Egypt, Centennial Meet. (Cairo), Abstr.*

GARSON, M.S. & KRS, M. (1976): Geophysical and geological evidence of the relationship of Red Sea transverse tectonics to ancient fractures. *Geol. Soc. Am., Bull.* **87**, 169-181.

GARUTI, G. & RINALDI, R. (1986): Mineralogy of melonite-group and other tellurides from the Ivrea–Verbano basic complex, western Italian Alps. *Econ. Geol.* **81**, 1213-1217.

GENKIN, A. (1971): Some replacement phenomena in copper–nickel sulfide ores. *Mineral. Deposita* **6**, 348-355.

GRATEROL, M. & NALDRETT, A.J. (1971): Mineralogy of the Marbridge No. 3. and No. 4 nickel–iron sulfide deposits, with some comments on low-temperature equilibration in the Fe–Ni–S system. *Econ. Geol.* **66**, 886-900.

GUILLON, J.C. (1975): Results of geophysical surveys carried out at Gabbro Akarem. *UNDP Tech. Rep. (Egypt).*

HAFEZ, A.M.A. & ABDEL-KADER, Z. (1982): Sulphides in the Gabbro Akarem complex, south- eastern desert, Egypt. *Precambrian Res.* **16**, A50-51.

HELMY, H.M., STUMPFL, E.F., MOGESSIE, A. & SHALABY, I.M. (1998): Platinum group minerals (PGM) in the Gabbro Akarem Cu–Ni deposits, south Eastern Desert, Egypt. *Abstr. 4th. Int. Conf. on Geology of the Arab World (Cairo).*

IRVINE, T.N. (1975): Crystallization sequences in the Muskox intrusion and other layered intrusions. II. Origin of chromitite layers and similar deposits of other magmatic ores. *Geochim. Cosmochim. Acta* **39**, 991-1020.

JAMES, R.S. & HAWKE, D. (1984): Geology and petrogenesis of the Kanichee layered complex, Ontario. *Can. Mineral.* **22**, 93-109.

KEAYS, R.R., ROSS, J.R. & WOOLRICH, P. (1981): Precious metals in volcanic peridotite-associated nickel sulfide deposits in western Australia. II. Distribution within the ores and host rocks at Kambalda. *Econ. Geol.* **76**, 1645-1674.

KHUDEIR, A.A., ABU EL RUS, M., HOINKES, G., MOGESSIE, A. & EL GABY, S. (1996): Petrogenesis of reversely zoned Gabbro Akarem mafic-ultramafic intrusion, south Eastern Desert, Egypt. *Geol. Surv. Egypt, Centennial Meet. (Cairo), Abstr.*

KRS, M. (1977): Rift tectonic development in the light of geophysical data, Red Sea region. *Studia Geophys. et Geod. (Prague)* **21**, 342-350.

KULLERUD, G. (1957): Phase relations in Fe–S–O. system. *Carnegie Inst. Wash., Year Book* **56**, 198- 200.

_____ (1967): Sulfides. *In* Researches in Geochemistry **2** (P.H. Abelson, ed.). John Wiley and Sons, New York, N.Y. (286-321).

LI, CHUSI, NALDRETT, A.J., RUCKLIDGE, J.C. & KILIUS, L.R. (1993): Concentrations of platinum- group elements and gold in sulfides from the Strathcona deposit, Sudbury, Ontario. *Can. Mineral.* **31**, 523-531.

MAKOVICKY, M., MAKOVICKY, E. & ROSE-HANSEN, J. (1986): Experimental studies on the solubility and distribution of platinum-group elements in base-metal sulfides in platinum deposits. *In* Metallogeny of Basic and Ultrabasic Rocks (M.J. Gallagher, R.A. Ixer, C.R. Neary & H.M. Prichard, eds.). Institute of Mining and Metallurgy, London, U.K. (415-425).

MISRA, K.C. & FLEET, M.E. (1973): The chemical compositions of synthetic and natural pentlandite assemblages. *Econ. Geol.* **68**, 518-539.

NALDRETT, A.J. (1969): A portion of the system Fe–S–O between 900 and 1080°C, and its application to sulfide ore magma. *J. Petrol.* **10**, 171-201.

_____ (1979): Partitioning of Fe, Co, Ni and Cu between sulfide liquid and basaltic melts and the composition of Ni–Cu sulfide deposits – a reply and further discussion. *Econ. Geol.* **74**, 1520-1528.

_____, ASIF, M., GORBACHEV, N.S., KUNILOV, V.E., FEDORENKO, V.A. & LIGHTFOOT, P.C. (1992b): The composition of the Ni–Cu ores of the Noril'sk region. *Can. Mineral.* **30**, 494-495.

_____, LIGHTFOOT, P.C., FEDORENKO, V., DOHERTY, W. & GORBACHEV, N.S. (1992a): Geology and geochemistry of intrusions and flood basalts of the Noril'sk region, USSR, with implications for the origin of the Ni–Cu ores. *Econ.Geol.* **87**, 975-1004.

NICKEL, E.H., ROSS, J.R. & THORNHER, M.R. (1974): The supergene alteration of pyrrhotite– pentlandite ore at Kambalda, Western Australia. *Econ. Geol.* **69**, 93-107.

PAULY, H. (1958): Igdlukunguaq nickeliferous pyrrhotite. *Medd. Grønland* **157**(3).

PELTONEN, P. (1995): Magma – country rock interaction and the genesis of Ni–Cu deposits in the Vammala Nickel Belt, SW Finland. *Mineral. Petrol.* **52**, 1-24.

RAMDOHR, P. (1969): *The Ore Minerals and their Intergrowths* (third ed.). Pergamon Press, London, U.K.

RASMY, A.H. (1982a): Mineralogy of copper–nickel sulfide mineralization at Akarem area, south Eastern Desert, Egypt. *Geol. Surv. Egypt Annals* **12**, 141-162.

_____ (1982b): Mackinawite from the copper–nickel prospect at Akarem area, south Eastern Desert of Egypt. *Geol. Surv. Egypt Annals* **12**, 177-184.

RIPLEY, E.M. (1990): Se/S ratios of the Virginia Formation and Cu–Ni sulfide mineralization in the Babbitt area, Duluth Complex, Minnesota. *Econ.Geol.* **85**, 1935-1940.

SHIMA, H. & NALDRETT, A.J. (1975): Solubility of sulfur in an ultramafic melt and the relevance of the system Fe–S–O. *Econ. Geol.* **70**, 960-967.

TAYLOR, L.A. & FINGER, L.W. (1970): Structural refinement and composition of mackinawite. *Carnegie Inst. Wash., Year Book* **69**, 318-322.

VAASJOKI, O., HÄKLI, T.A. & TONTTI, M. (1974): The effect of cobalt on the thermal stability of pentlandite. *Econ. Geol.* **69**, 549-551.

WILSON, G.C. (1998): Economic applications of accelerator mass spectrometry. *In* Applications of Microanalytical Techniques to Understanding Mineralizing Processes (M.A. McKibben, W.C. Shanks & W.I. Ridley, eds.). *Rev. Econ. Geol.* **7**, 187-198.

_____, KILIUS, L.R. & RUCKLIDGE, J.C. (1995): Precious metal contents of sulfide, oxide and graphite crystals: determinations by accelerator mass spectrometry. *Econ. Geol.* **90**, 255-270.

_____, _____, _____, DING, GANG-JIAN & ZHAO, XIAO-LEI (1997): Trace-element analysis of mineral grains using accelerator mass spectrometry – from sampling to interpretation. *Nucl. Instrum. Methods Phys. Res.* **B123**, 579-582.

_____, ZHAO, XIAO-LEI, RUCKLIDGE, J.C. & SHARARA, N.A. (1998): Automated analysis of precious metals in Egyptian sulphides. *In* IsoTrace Laboratory 1996 Annual Report (G.C. Wilson, ed.), University of Toronto, Toronto, Ontario (29-31).

YUND, R.A. & HALL, H.T. (1969): Hexagonal and monoclinic pyrrhotites. *Econ. Geol.* **64**, 420-423.

_____ & KULLERUD, G. (1966): Thermal stability of assemblages in the Cu–Fe–S system. *J. Petrol.* **7**, 454-488.

Received January 8, 1999, revised manuscript accepted September 25, 1999.